Princeton Plasma Physics Laboratory

PPPL- 4876

PPPL- 4876

Collisionality Scaling of Main-ion Toroidal and Poloidal Rotation in Low Torque DIII-D Plasmas

B.A. Grierson,. K.H. Burrell, W.M. Solomon, R.V. Budny and J. Candy

May, 2013

PPPL PRINCETON PLASMA PHYSICS LABORATORY

Prepared for the U.S. Department of Energy under Contract DE-AC02-09CH11466.

Princeton Plasma Physics Laboratory
Report Disclaimers

Full Legal Disclaimer

Trademark Disclaimer

PPPL Report Availability

Princeton Plasma Physics Laboratory:

http://www.pppl.gov/techreports.cfm

Office of Scientific and Technical Information (OSTI):

http://www.osti.gov/bridge

Related Links:

U.S. Department of Energy

Office of Scientific and Technical Information

Fusion Links

Collisionality Scaling of Main-ion Toroidal and Poloidal Rotation in Low Torque DIII-D Plasmas

B.A. Grierson[1], K.H. Burrell[2], W.M. Solomon[1], R.V. Budny[1], and J. Candy[2]

[1]Princeton Plasma Physics Laboratory, Princeton University, Princeton, NJ 08543, USA

[2]General Atomics, P.O. Box 85608, San Diego, CA 92186-5608, USA

E-mail: bgriers@pppl.gov

Abstract. In tokamak plasmas with low levels of toroidal rotation, the radial electric field E_r is a combination of pressure gradient and toroidal and poloidal rotation components, all having similar magnitudes. In order to assess the validity of neoclassical poloidal rotation theory for determining the poloidal rotation contribution to E_r, D_α emission from neutral beam heated tokamak discharges in DIII-D [J.L. Luxon, Nucl. Fusion **42**, 614 (2002)] has been evaluated in a sequence of low torque (electron cyclotron resonance heating and balanced diagnostic neutral beam pulse) discharges to determine the local deuterium toroidal rotation velocity. By invoking the radial force balance relation the deuterium poloidal rotation can be inferred. It is found that the deuterium poloidal flow exceeds the neoclassical value in plasmas with collisionality $\nu_i^* < 0.1$, being more ion diamagnetic, and with a stronger dependence on collisionality than neoclassical theory predicts. At low toroidal rotation, the poloidal rotation contribution to the radial electric field and its shear is significant. The effect of anomalous levels of poloidal rotation on the radial electric field and cross-field heat transport is investigated for ITER parameters.

Submitted to: *Nucl. Fusion*

1. Introduction

The radial electric field in a tokamak plasma, and associated $\mathbf{E} \times \mathbf{B}$ shear, provides stabilization of long wavelength turbulent modes and improves plasma confinement [1, 2]. In order to predict the heat transport and fusion performance in ITER, the $\mathbf{E} \times \mathbf{B}$ shearing rate is required to compare with turbulent growth rates and determine the effective suppression of cross-field heat transport driven by turbulent fluctuations. Through the radial force balance relation, the radial electric field is a combination of three terms, with dependencies on the pressure gradient, toroidal rotation and poloidal rotation $E_r = \nabla P/Zen_i + V_\varphi B_\theta - V_\theta B_\varphi$, where ∇P is the ion pressure gradient, Ze the ion charge, n_i the ion density and V_φ, V_θ, B_φ, B_θ being the toroidal (φ) and poloidal(θ) velocities and magnetic fields, respectively. In tokamak discharges heated by uni-directional neutral beams, the high toroidal rotation produces a large radial electric field and $\mathbf{E} \times \mathbf{B}$ flow shear that suppresses turbulent transport [1]. As toroidal rotation is lowered by reduced net torque, the benefit of the large shearing rate provided by rapid toroidal rotation decreases [3]. Predictions of ITER with GLF23 [4, 5] and the more recent TGLF [6] indicate a significant increase in fusion performance with increased $\mathbf{E} \times \mathbf{B}$ shear, however in devices with low relative torque the benefits of the large toroidal rotation may be absent. The core E_r will be determined by the contributions from the pressure gradient, toroidal rotation and poloidal flow, all having similar magnitude [7]. Although the poloidal flow is generally considered small, in a conventional tokamak (in contrast to a spherical torus) V_θ enters into the radial electric field multiplied by the large B_φ. Predictions of E_r and plasma performance in future devices rely on calculations and simulations of the main-ion properties ($V_\varphi, V_\theta, \nabla P_i$ and E_r derived from these values) [7], hence an understanding of the main-ion toroidal and poloidal flows is required when evaluating E_r. For ITER design parameters [I_p, B_t, neutral beam injection (NBI) all clockwise from above], the contributions to E_r from NBI-driven toroidal rotation and ion-diamagnetic poloidal rotation add in a positive sense ($E_r^{V_\varphi}, E_r^{V_\theta} > 0$), while the pressure gradient opposes these terms ($E_r^{\nabla P} < 0$). Therefore both large toroidal and poloidal rotation will increase the core radial electric field, and its shear. Indeed on JET [8], an anomalously large poloidal rotation was observed to have a significant effect on the core radial electric field, and was determined to play a significant role in the formation of core transport barriers.

Poloidal rotation in tokamaks is strongly damped by the time variation of the magnetic field seen in the rest frame of poloidally passing ions [9] (trapped particles carry no net poloidal momentum). In the absence of poloidal momentum sources, the damping rate of poloidal flow can be determined by the flux surface averaged parallel stress $\langle \mathbf{B} \cdot \nabla \cdot \mathbf{\Pi} \rangle$ [10], which damps poloidal flow to the neoclassical level on an ion-ion collision time. Poloidal flow can be modified ("spin-up") by steady-state poloidal density asymmetries [11] or poloidally-asymmetric particle or momentum injection [12]. Additionally, turbulent generation of mean-field poloidal flow may be driven by Reynolds stress when there is a radial gradient in the radial and poloidal velocities associated with

the fluctuating electrostatic potential [13, 14, 15, 16, 17, 18].

Poloidal flow of main-ions and impurities should be quite different, as the magnetic pumping damps its own species [19] with a parallel viscosity proportional to collision frequency $\mu_{ii} \propto \nu_{ii}$ that is larger for the more collisional impurity ions. It is this fact that makes validation of the neoclassical theory a challenge for experimentalists, as the impurity ions are measured much more commonly than the main-ions, but are predicted to have much smaller magnitude flow velocities. Additionally, the neoclassical theory of impurity poloidal rotation has three significant drive terms; main-ion temperature and pressure gradient and impurity pressure gradient, whereas the main-ion poloidal flow is dominated by the temperature gradient alone [19, 20], which would greatly simplify designing experimental tests of the theory. In many cases, aside from strong core transport barriers, the neoclassical prediction of impurity poloidal rotation is quite small and near the resolution level of the diagnostic designed for the measurement. Early accounts of poloidal rotation contained zero within the error bars of the measurements [21], but through sophisticated atomic calculations [22, 23] and novel diagnostic viewing configurations [24, 25, 26] the measurements uncertainties have been reduced to such levels that the poloidal flow theory may be tested.

Experimental measurements of poloidal rotation have displayed a mix of agreement and disagreement with neoclassical estimates. Here we neglect disagreement with neoclassical theory prior to 2000 cf. reference [27]. Measurements on MAST [20] and TCV [25] have displayed impurity poloidal rotation that is considered neoclassical within the error bars. These tests have been done in plasmas with relatively low ion temperatures, and hence in higher collisionality than fusion relevant conditions. A recent test of neoclassical poloidal rotation was done by Bell, *et al.* on NSTX [28]. Here the measured impurity poloidal rotation was near neoclassical estimates, but smaller in magnitude. Smaller magnitude here means that the flow was more *ion diamagnetic* than neoclassical in all cases, and as the toroidal field was lowered, the measured flow displayed a larger discrepancy with neoclassical, again being more *ion diamagnetic*. Here ion diamagnetic means the direction of $\mathbf{B} \times \nabla P$. Work on the DIII-D tokamak in high performance QH and H-mode plasmas displayed significant disagreement with neoclassical theory, in both sign and magnitude. In all cases reported in reference [23], the impurity poloidal flow was more *ion diamagnetic* than neoclassical. Previous measurements of the main-ion differential toroidal rotation on DIII-D displayed an inference of the main-ion poloidal rotation that was more *ion diamagnetic* than neoclassical [29], and an experimental database of observations are the subject of this paper. Although flow in the H-mode pedestal is beyond the scope of this paper, the poloidal rotation of helium main-ions near the separatrix have also been seen as significantly more *ion diamagnetic* than neoclassical, approaching 30% of the ion diamagnetic velocity [30]. A newly developed diagnostic for measuring the core poloidal rotation, that in principle has higher accuracy than previous techniques, has recently been commissioned on DIII-D and has reported poloidal flow that is near neoclassical, but somewhat more *ion diamagnetic* [26].

The primary difference between this and previous studies is that we are experimentally investigating the main-ion poloidal rotation in deuterium plasmas. This is only currently possible by directly measuring the toroidal rotation, and using the force balance relation. This article further investigates the main-ion toroidal and poloidal contributions to E_r, and the studies are done under low rotation conditions in DIII-D. Plasmas are either ohmic or H-mode heated by electron cyclotron heating (ECH), with short NBI pulses used for diagnostic purposes. Thus the regime considered here is well represented by $T_e \approx T_i$ and $n_b \ll n_e, n_D$, where n_b is beam ion density and n_e, n_D are electron and deuterium density, respectively. Main-ion [29, 31] and impurity [32, 33, 34] charge exchange recombination (CER) spectroscopy are used to measure the toroidal rotation of the deuterium and carbon ions, as well as the impurity poloidal flow velocity [22, 23]. Neoclassical theory is used to predict the carbon and deuterium poloidal rotation and the deuterium toroidal rotation. By comparing the measured toroidal rotational velocities, and using the radial force balance relation, the main-ion poloidal rotation can be inferred and compared to the neoclassical values. We exploit the fact that the impurity poloidal rotation in these conditions is both predicted and measured to be small, and hence little bias on the inferred main-ion poloidal rotation is introduced by using the carbon measurements. Comparisons between measurements and neoclassical models are done by forward modeling with neoclassical codes, as well as deducing the fundamental neoclassical quantities (V_θ and coefficients depending on collisionality) through the force balance relation. The second method permits a straightforward propagation of errors in experimental profiles and gradients.

We find that the core main-ion poloidal flow exceeds standard neoclassical estimates from the NCLASS [35] model, being significantly larger in the ion diamagnetic direction. When E_r is evaluated with the main-ion constituents, we find that the poloidal rotation contribution dominates over the toroidal rotation, and the sum enhances the core radial electric field to a value larger than neoclassical estimates. A database of discharges has been evaluated, and a consistent trend has been exposed indicating a significantly larger poloidal flow at low collisionality than conventional neoclassical theories predict.

2. Neoclassical Theory

Neoclassical theory provides an expected poloidal flow, given the magnetic equilibrium and plasma profiles [19]. Neoclassical poloidal flow of the main-ions is largely driven by the temperature gradient, with a coefficient K_1 that depends on collisionality

$$V_\theta = K_1 \frac{v_{Ti}\rho_i}{2L_{Ti}} \frac{BB_\varphi}{\langle B^2 \rangle} \quad , \tag{1}$$

where v_{Ti} is the ion thermal speed, ρ_i is is the gyro-radius, L_{Ti} is the ion temperature scale length ($T_i/\nabla T_i$), B_φ is the toroidal magnetic field, B is the total magnetic field, and $\langle\ \rangle$ denotes a flux-surface average. Here K_1 is formed by evaluating the impurity concentration and parallel viscous matrix elements. Calculations of the coefficient

K_1 can be done analytically [19], numerically [35, 36], or determined from plasma simulations [37, 38, 39].

In the infinite aspect ratio ($\epsilon \to 0$), pure plasma collisionless limit, the coefficient $K_1 \to 1.17$. This banana limit corresponds to main-ion poloidal flow in the ion diamagnetic direction. For higher collisionality plateau ($\nu_i^* > 1$) and Pfirsch-Schlüter ($\nu_i^* > \epsilon^{-3/2}$) regimes the coefficient changes sign and magnitude to -0.5 and -1.0 respectively. For intermediate aspect ratios K_1 decreases in magnitude but remains positive in the banana regime. Impurity poloidal flow is generally smaller than the main-ion flow, but is more commonly measured [20, 23, 28, 40, 41]. Impurity poloidal flow can be expressed as

$$V_\theta^{imp} = \frac{\upsilon_{Ti}\rho_i}{2}\Big[\Big(K_1 + \frac{3}{2}K_2\Big)L_{Ti}^{-1} - L_{Pi}^{-1} + \frac{Z_i T_{imp}}{Z_{imp}T_i}L_{Pimp}^{-1}\Big]\frac{BB_\varphi}{\langle B^2\rangle} \quad , \tag{2}$$

where subscripts i and imp denote primary and impurity ions, respectively, and L_P is the pressure gradient scale length. Impurity poloidal flow largely depends on main-ion parameters due to the Z_i/Z_{imp} dependence. Poloidal flow can be modified from the neoclassical treatment by the turbulent Reynolds stress $V_\theta^{RS} = -\nabla\cdot\mathbf{\Pi}_{r,\theta}^{RS}/\mu_{ii} = -\mu_{ii}^{-1}\partial\langle\tilde{v}_r\tilde{v}_\theta\rangle/\partial r$ [13, 15, 42], where μ_{ii} is the ion viscosity and $\tilde{v}_r, \tilde{v}_\theta$ are the radial and poloidal $\mathbf{E}\times\mathbf{B}$ velocities associated with a fluctuating electrostatic potential. The turbulent contributions effectively add to the neoclassical level, $V_\theta = V_\theta^{NC} + V_\theta^{RS}$ (See revised calculations of reference [43] in reference [44].). Non-local effects and inclusion of the radial electric field can also provide a modification to the standard neoclassical prediction of poloidal rotation values [38, 45].

In this paper we make use of a number of neoclassical models. The first model that can be evaluated is the analytic Kim-Diamond-Groebner model (KDG) [19]. The KDG model can be readily evaluated in post-processing of routine experimental profile analysis. The second model is the NCLASS model, evaluated through the FORCEBAL pre-processor [35, 46]. Typical NCLASS evaluation retains the full viscosity coefficients that are valid across all collisionality regimes and aspect ratios(as was done previously in references [23, 46]), but can also be evaluated neglecting the high collisionality, Pfirsch-Schlüter viscosity. Neglecting the Pfirsch-Schlüter viscosity effectively increases the poloidal flow coefficient K_1, but decreases the differential poloidal flow between species. The third model is NEO [36], a δf Eulerian model that solves the drift-kinetic equation in a multi-ion species plasma. The fourth model is GTC-NEO [38, 45], a δf particle-in-cell (PIC) code that solves the drift-kinetic equation by evolving a finite number of particles based on the Lagrangian equation. Each neoclassical simulation (FORCEBAL-NCLASS, GTC-NEO and NEO) is executed with the default settings for the respective code. Some differences between the codes are the treatment of orbit squeezing effects and the inductive parallel electric field. Orbit squeezing modifications to the viscosity are not used in either FORCEBAL-NCLASS or NEO, but are included self-consistently in the particle-following GTC-NEO and have been shown to affect the ion poloidal rotation [39]. FORCEBAL-NCLASS by default includes an inductive parallel electric field $E_\parallel$ by assuming neoclassical resistivity for the ohmic current, whereas GTC-NEO

and NEO by default have chosen to set the parallel inductive field to zero, as $E_\parallel$ is a difficult quantity to determine accurately. A comparison of the various options for each simulation such as orbit-squeezing, potato orbits near the magnetic axis, sensitivity to a parallel electric field and other such effects are beyond the scope of this study, and are left to future benchmarking. For all simulations, toroidal rotation of the main-ion species is predicted by adding the pressure and poloidal rotation contributions to E_r, giving $V_\varphi^D = V_\varphi^C + B_\theta^{-1}(E_r^{\nabla P_C} - E_r^{\nabla P_D}) + B_\theta^{-1}(E_r^{V_\theta^C} - E_r^{V_\theta^D})$, where the only quantities used from the neoclassical models are V_θ^C and V_θ^D used in $E_r^{V_\theta} = -V_\theta B_\varphi$.

As will be seen in the following section, the choice of neoclassical model can have significant effects on the magnitude of the predicted poloidal rotation, varying by nearly a factor of two. Thus the evaluation of agreement or disagreement with neoclassical theory depends on which model is chosen to represent that theory.

3. Experimental Method

A sequence of discharges were performed in DIII-D to investigate the intrinsic rotation characteristics of the main-ions and impurities using the newly commissioned main-ion CER system [31]. The discharges were executed by Ohmic startup, with a single short beam pulse for diagnostic purposes. Plasma current and toroidal field were varied between 0.7–1.1 MA and -1.7, -2.0 T on a shot-by-shot basis. Diagnostic pulses provide core ion temperature, main-ion and carbon toroidal rotation, carbon poloidal rotation and carbon density. Second harmonic ECH (X-mode) of 0.9 MW was applied to trigger the low to high (L-H) confinement transition and enter edge localized mode (ELM) -free H-mode. During the H-mode phase, diagnostic beam pulses were applied to obtain the spectroscopic measurements at three more times. Diagnostic beam pulses were designed to impart zero net torque by usage of co- and counter-current NBI.

Early ohmic conditions have the lowest ion temperature ($T_i \sim 1.0$ keV) and highest collisionality, with line-averaged density approximately $\langle n_e \rangle = 3 \times 10^{19}$ m^{-3}. H-mode temperatures reach $T_i \sim 2.0$ keV with line-averaged density of $\langle n_e \rangle = 5.5 \times 10^{19}$ m^{-3}. No significant MHD or other instabilities such as ELMs or sawteeth were observed. During ECH a reversal of the q profile develops for $\rho_{qmin} \approx 0.2 - 0.3$. Profiles of ion temperature in H-mode develop a steepened gradient inside of $\rho \sim 0.4$, and the carbon density in this region is reduced.

One example of the plasma conditions during the ECH H-mode is provided in figure 1(a,b). Here the profiles of electron, deuterium, and carbon density are displayed as a function of flux-surface label, $\rho = \sqrt{\psi_t/\pi/B_{center}}$, where ψ_t is toroidal flux and B_{center} is defined at the magnetic axis, normalized to the value at the boundary. In all cases, error bars on the experimental profiles are obtained from Monte-Carlo perturbations within the experimental data points. Ion temperature is obtained from CER and electron temperature is obtained from Thomson scattering and ECE. Figure 1(c) presents the measured carbon and deuterium toroidal rotation from the two spectroscopy systems. Here the values of toroidal rotation are outboard-midplane

measurements. The carbon toroidal rotation possesses a feature that is hollow in the same region of the plasma as the hollow carbon density profile, apparently caused by ECH. The deuterium toroidal rotation profile is slightly slower than carbon at outer locations, and faster at $\rho \approx 0.25$. Also included in figure 1(c) is the predicted toroidal rotation profile of the deuterons from the NCLASS code [35]. This NCLASS analysis includes all viscosity contributions. It can be seen that the NCLASS prediction is significantly faster in the toroidal direction (direction of plasma current) than the measured deuterium rotation. This difference, $(V_\varphi^D - V_\varphi^C)$ is presented in figure 1(d), as well as predictions from two other neoclassical models; Kim-Diamond-Groebner, and NEO.

The neoclassical quantity required for the prediction of V_φ^D is the difference $V_\theta^D - V_\theta^C$. Using radial force balance, we can define ΔV_θ as

$$(V_\theta^D - V_\theta^C) = \frac{1}{B_\varphi}\Big(\frac{\nabla P_D}{Z_D e n_D} - \frac{\nabla P_C}{Z_C e n_C}\Big) + \frac{B_\theta}{B_\varphi}(V_\varphi^D - V_\varphi^C). \tag{3}$$

The terms on the RHS of equation (3) are readily evaluated from the equilibrium reconstruction and experimental measurements and do not rely on any theoretical predictions. The LHS of equation (3) is then defined as ΔV_θ^{exp} and will be used for comparison to the neoclassical theory.

Neoclassical calculations produce V_θ^D and V_θ^C individually on the outboard midplane, and the quantity ΔV_θ^{NC} can be formed from calculations and simulations. Thus this differential poloidal flow velocity is the clearest comparison to the neoclassical theory of poloidal rotation that *does not depend on the measurement of poloidal velocity.* Comparison of ΔV_θ^{exp} to ΔV_θ^{NC} displays how quickly poloidally passing main ions and impurity ions move past each other, regardless of any common poloidal flow that may exist for the two ion species. The results from experimental profiles and neoclassical theory are presented in figure 2(a) for the same ECH H-mode displayed in figure 1. The experimental and neoclassical models all display the same qualitative feature, namely a peak in the differential flow velocity at the location of the largest ion temperature gradient. By examining the various models, we see that the KDG analytic model produces the smallest differential poloidal flow, followed by the NCLASS model with full viscosity evaluation, NEO and GTC-NEO. It is the NCLASS profile in figure 2(a) that was used to produce the toroidal rotation profile in figure 1(c). The fact that the NCLASS ΔV_θ^{NC} is approximately 2 km/s below the observation is manifested as a peak 18 km/s difference in predicted toroidal flow. This is due to the factor of B_φ/B_θ in the equation for differential toroidal flow. The GTC-NEO model produces the largest differential poloidal flow at the location of the steep temperature gradient.

We can arrive at an inferred main-ion poloidal flow velocity by using the experimental measurements of the carbon poloidal velocity; $V_\theta^D = V_\theta^C + \Delta V_\theta^{exp}$. The experimentally measured carbon poloidal flow is displayed in figure 2(b), along with the neoclassical calculations from the various models. Under these conditions, the diagnostic difficulties associated with impurity poloidal rotation are reduced compared to rapidly rotating plasmas because there is little "toroidal pickup", as the toroidal rotation is

only tens of km/s, and the ion temperature is quite low. Here "toroidal pickup" is defined as the contribution to a vertical (poloidal) velocity due to toroidal rotation when the angle between a vertical sightline and the toroidal direction is not exactly perpendicular. As expected, the measured and predicted carbon flow velocities are very small, and nearly zero within the error bars. The NCLASS model for V_θ^C displays a strong electron diamagnetic feature at $\rho \approx 0.2$, with the other two models, NEO and GTC-NEO displaying a weaker feature. However, this feature is not observed experimentally. It is noteworthy that the measured impurity poloidal flow is more ion diamagnetic than the neoclassical models in the region of steep pressure. For the conditions in figure 1, the main-ions are in the banana collisionality regime across the entire core profile ($\nu_i^* \approx 0.05$), while carbon enters the plateau regime at $\rho \approx 0.5$. Thus we expect the main-ion poloidal flow to be ion diamagnetic, as displayed in figure 2(c), and largest at the location of steepest temperature gradient. However, and similar to previous investigations, the inferred deuterium poloidal rotation is more ion diamagnetic than neoclassical predictions. $K_1^{exp}(\rho)$ (not shown) is consistent with expectation, being approximately 1.0 at the location of smallest collisionality. The NEO and NCLASS models are somewhat below this limit ($K_1 \approx 0.8, 0.3$, respectively), where NCLASS presents the smallest value. By neglecting Pfirsch-Schlüter viscosity in the NCLASS evaluation, the value of K_1 increases uniformly to $K_1 \approx 0.5$. The radial electric field is displayed in figure 2(d,e). At the location of the steepest ion temperature gradient, the core E_r is enhanced above the NCLASS estimate by approximately a factor of two. By examining the contributions to E_r from main-ion properties, it is clear that the poloidal rotation contribution is not negligible. Inside of ρ of 0.4, the poloidal rotation dominates over the toroidal rotation term and is comparable in magnitude to the pressure gradient term.

4. Scaling trends

In the sequence of discharges performed to investigate main-ion and impurity intrinsic rotation, the variation in plasma current naturally causes changes in plasma density, temperature and collisionality. Thus, a database of measured differential toroidal and poloidal flow, and inferred main-ion poloidal flow, can be used to expose trends in the data and compare to expected trends in the theory. For each time in each discharge, an MSE-constrained, kinetic equilibrium reconstruction was performed using plasma profiles and ONETWO [47] transport analysis to obtain the q profile and magnetic axis location. For each set of equilibria and profiles, the carbon poloidal rotation was determined by the method detailed in references [22, 23], accounting for the energy dependence and gyro-orbit cross-section effects on the apparent velocity. Each equilibrium and set of profiles were evaluated with NCLASS.

First, the trends in the difference between direct measurements of deuterium and carbon toroidal rotation are investigated. We display the difference in toroidal rotation $V_\varphi^D - V_\varphi^C$ averaged over $\rho = [0.2, 0.7]$ in figure 3. It can be seen that NCLASS always

predicts this quantity as positive, i.e. deuterium is predicted to rotate more co-current than carbon, and trends more positive at lower collisionality, where the temperatures are higher and the pressure profile more peaked. The measured difference in toroidal rotation is only positive at the highest collisionality, and trends more *negative* at lower collisionality. As will be shown later in this section, this discrepancy between theory and experiment, that appears initially as a sign error, can be explained by a simple increase of the magnitude of main-ion poloidal rotation in the *ion diamagnetic* direction, at low collisionality.

By using the differential toroidal rotation displayed in figure 3, we can then calculate the differential poloidal rotation. We compare this quantity ΔV_θ^{exp} and ΔV_θ^{NC} to the neoclassical theory because this quantity does not require the more complicated measure of carbon poloidal rotation. However, the differential poloidal rotation does not provide a scaling of the absolute main-ion poloidal flow, which would be beneficial to predictions of E_r and $\mathbf{E}\times\mathbf{B}$ suppression of turbulence on future devices. Therefore, in order to make progress we must also form the main-ion poloidal flow by adding the measured poloidal rotation of carbon to ΔV_θ^{exp}, and computing the dimensionless poloidal flow coefficient, K_1^{exp}. This coefficient is also computed from the neoclassical models either directly (as in the case of KDG), or numerically by inverting the equation $V_\theta^D = (K_1/m_i\Omega_{ci})\nabla T_i$ for K_1^{NC} on the outboard midplane. Here collisionality is defined as the ratio of ion-ion collision frequency to bounce frequency, $\nu_i^* = \nu_{ii}Rq/\epsilon^{3/2}v_{th,i}$.

In order to expose scaling trends in the sequence of discharges, we evaluate the quantities ΔV_θ^{exp}, ΔV_θ^{NC}, V_θ^D and K_1 over a relatively large fixed range in $\rho = [0.2, 0.7]$, providing a general impression of the core poloidal flow properties. Figure 4(a) displays the trend in the differential poloidal flow obtained from experimental measurements, as well as differential poloidal flow from neoclassical calculations. Error bars here represent the error in the velocities as well as the collisionality range covered by the radial region. It is stressed that this experimental quantity does not depend on the direct measure of the impurity poloidal flow. From figure 4, we see a strong increase in the differential poloidal flow at low collisionality. This scaling trend is expected, because the strongest drive for the differential poloidal flow is the ∇T_i that naturally increases at low collisionality for these discharges conditions. The experimental ΔV_θ exhibits a stronger scaling than the NCLASS evaluation as collisionality decreases. A simple offset would not account for the observed mismatch with the theory. Subtracting the offset would still result in a factor of two difference at $\nu_i^* \approx 0.05$. By adding the carbon poloidal rotation measurement, we calculate and display the main-ion poloidal flow velocity, seen in figure 4(b). As with the observed trends in the differential toroidal and poloidal flow, at low collisionality the discrepancy with neoclassical becomes larger. Here we point out that what appears to be a significant change in both sign and trend in differential toroidal flow, figure 3, is resolved by a "spin-up" of main-ion poloidal flow in the ion diamagnetic direction.

Differential poloidal rotation has a strong dependence on the temperature gradient, and this dependence is removed by displaying the dimensionless poloidal flow coefficient

K_1 as a function of ν_i^*, presented in figure 5. An error band was formed by Monte-Carlo linear fits with error bars on both K_1 and ν_i^*, and the shaded region falls inside of one-sigma. Scaling of K_1 for experimental measurements and NCLASS are approximately linear and show an increase in K_1 as collisionality is lowered. Experimental values are larger than NCLASS at low collisionality, and display a stronger slope across the range of ν_i^* in these discharges. An additional measurement point is introduced in figure 5 at the lowest collisionality that was taken from a distinctly different set of discharge conditions, and first presented in reference [29] during the formation of a strong core transport barrier in a strongly NBI heated plasma with both co- and counter-I_p injection. The data point presented is consistent with the scaling trend observed in the rest of the database.

The implications are that main-ion poloidal flow is significantly more ion diamagnetic than NCLASS predictions as the collisionality approaches zero. Neglecting the Pfirsch-Schlüter contributions to the viscosity produces a K_1 from NCLASS that is more positive, but not to observed levels. Scaling results from the GTC-NEO code are left to a future exercise, as the computational time is prohibitive.

The scaling trends in figure 4 are consistent with the reasonable agreement demonstrated in other devices at higher collisionality [20, 25], and the disagreement at lower collisionality [8, 23]. Data at higher collisionality are more difficult to obtain as it requires very low ion temperatures. The inherent error bars on the measurements will dominate over the extremely low level of poloidal flow expected under those conditions, and the high collisionality regime is irrelevant to high performance plasmas. At low collisionality the poloidal flow is enhanced, and this is consistent with an increased turbulent drive. Turbulent poloidal flow generation should increase at low collisionality, as $V_\theta^{tur} \sim \mu_{ii}^{-1}$, where $\mu_{ii} \sim \nu_{ii}$.

Future experiments in helium main-ion plasmas with deuterium neutral beams offer a further test of the neoclassical theory, as outlined in this manuscript. It has been noted that the toroidal rotation of helium ions in intrinsic rotation conditions with carbon impurity also disagreed with the neoclassical estimates [48], and a database similar to the one presented in this paper could be formed that uses both the differential toroidal flow, as well as the direct measure of helium poloidal rotation.

5. Discussion of effect anomalous poloidal rotation has on $\mathbf{E} \times \mathbf{B}$ shear rates in ITER-relevant conditions

Enhanced poloidal rotation above the NCLASS neoclassical level directly affects the radial electric field. In order to assess the effect of enhanced V_θ on $\mathbf{E} \times \mathbf{B}$ shearing rates, an ITER scenario will be investigated to determine possible consequences if the experimental scaling presented in figure 5 is relevant to plasmas expected in ITER. This investigation will ignore speculation on turbulent generation of poloidal rotation and any ρ^* scaling of such effects. Predictive transport run 20100N05 at 245 seconds has been investigated recently [49] for predictions of ITER performance with

coupled PTRANSP [5, 7]-TGLF [50], and contrasted with previous predictions using GLF23 [4, 51]. The results of Budny *et al.* [49] displayed prediction of core T_e, T_i with a higher sensitivity to the $\mathbf{E}\times\mathbf{B}$ shearing rate than previous GLF23 simulations, hence modifications to the core E_r will be more pronounced within the new, more accurate TGLF modeling.

Two profiles of E_r are given in figurre 6(a,b). figure 6(a) displays the radial electric field evaluated by the deuterium pressure, toroidal and poloidal flows and used in the PTRANSP simulation. The toroidal rotation was computed by the injected neutral beam torque, and the assumption that $\chi_\phi/\chi_{i,GLF23} = 0.5$, resulting in a peak rotation of approximately 75 km/s at $R = 6.8\,\mathrm{m}$. Poloidal rotation was computed using NCLASS, and under these low collisionality conditions the the dimensionless flow coefficient is $K_1^{NC} \approx 0.5$ across much of the core profile, consistent with the NCLASS scaling in figure 4(b) at very low ν_i^*. By enhancing the poloidal rotation in accordance to the scaling trend observed experimentally, assuming $K_1 = 2.0$, the effect on the core radial electric field can be determined and used in assessing the enhancement of E_r, seen in figure 6(b). It can be seen that the magnitude of E_r in increased across the entire core plasma.

Here we compute the long wavelength ion growth rates from TGYRO-TGLF in the linear stability mode of the simulation. The reported growth rate is γ_i where $\gamma_i/(k_y\rho)^2$ is maximized, typically near $k_y\rho = 0.3$. This is compared against the $E\times B$ shear rate, where we define here the familiar Hahm-Burrell shear rate and the Waltz-Miller rate

$$\gamma^{HB}_{\mathbf{E}\times\mathbf{B}} = \frac{(RB_\theta)^2}{B}\frac{\partial}{\partial\psi}\Big(\frac{E_r}{RB_\theta}\Big) \quad , \tag{4}$$

$$\gamma^{WM}_{\mathbf{E}\times\mathbf{B}} = -\frac{r}{q}\frac{\partial\omega_0}{\partial r} \quad , \tag{5}$$

where R is major radius, B_θ is the poloidal field, B is the total field and ψ is the poloidal flux. For the Waltz-Miller form, $\omega_0 = -c\partial\phi_{-1}/\partial\psi$ is a flux-function and is the $\mathbf{E}\times\mathbf{B}$ rotation, locally E_r/RB_θ on the outboard midplane. Displayed in figure 7 are the turbulent growth rates and shearing rates across the outboard midplane, where both forms of the shearing rate are presented (Hahm-Burrell and Waltz-Miller). Two cases of calculated shearing rate are included in figure 7, derived from the original E_r profile with NCLASS poloidal rotation, and the modified E_r with poloidal rotation enhanced above the neoclassical value with coefficient $K_1 = 2.0$. It can be seen that the modified shearing rate is above the original shear rate, and that over a significant fraction of the core profile ($R \lesssim 7.4$ m) that the $\mathbf{E}\times\mathbf{B}$ shear rate with modified poloidal rotation equals or exceeds the linear turbulent growth rate.

When local $\mathbf{E}\times\mathbf{B}$ shear rates approach and exceed the linear turbulent growth rates, the turbulent transport can be suppressed [1]. In order to asses the effects of the enhanced poloidal rotation on the temperature profiles, the TGYRO [52] framework with TGLF has been employed to produce self-consistent steady-state ion and electron temperature profiles for the this ITER scenario. TGYRO here utilizes the ITER geometry and heating sources to predict the ion and electron temperature

profiles consistent with neoclassical and turbulent transport. At each grid point in the simulation, the flux-matching gradients are predicted, which in turn determines the temperature profile. The simulation has the profiles fixed at a reference minor radius (here $r/a = 0.84$, $R \approx 7.9$ m, inside of the pedestal) and interior points are predicted by TGYRO. Toroidal rotation prediction from TGYRO-TGLF is currently undergoing validation, and therefore we suppress any evolution of the toroidal rotation profile in these simulations and retain the assumed toroidal rotation profile from the original PTRANSP simulations. A self-consistent evolution of the equilibrium, temperature, density and rotation profiles of all species is beyond the scope of the present investigation and is left to future work.

Ion and electron temperature profiles from the TGYRO analysis are given in figure 8 for a scan in poloidal flow coefficient from the original NCLASS and $K_1 = 1.0, 1.5, 2.0$. Ion temperature profiles from the simulations begin to diverge near $R \approx 7.1$ m. At this location, the relationship between the growth and shearing rates (figure 7) qualitatively change. For $R \gtrsim 7.3$ m the turbulence growth rate exceed the $\mathbf{E} \times \mathbf{B}$ shear rates $\gamma_{\mathbf{E}\times\mathbf{B}}$, $\gamma^{mod}_{\mathbf{E}\times\mathbf{B}}$. For $R \lesssim 7.3$ m the modified shear rate approaches or exceeds the turbulence growth rates, while the original shear rate is below the ion growth rate, $\gamma^{mod}_{\mathbf{E}\times\mathbf{B}} > \gamma_i > \gamma_{\mathbf{E}\times\mathbf{B}}$. Enhanced shear causes a decrease of the turbulent heat flux, and an increase of the ion temperature by approximately 25% is seen at the magnetic axis for the case with $K_1 = 2.0$. The effect on the electron temperature profile is qualitatively similar, but the enhancement to T_e is weaker (9%). Although the plasma volume decreases towards the magnetic axis, raising the central ion temperature by 25% will result in an increase in fusion power. Volume integrated alpha power for $K_1 = 2.0$ is approximately 15% higher than the NCLASS case.

This investigation of the effects of anomalous poloidal rotation in ITER-relevant conditions motivates future study of main-ion toroidal and poloidal rotation properties in deuterium and D-T plasmas.

6. Conclusion

A series of discharges were executed with the aim to determine the intrinsic rotation properties on main-ions and impurity ions in the DIII-D tokamak. Measurements of the toroidal rotation of main-ions and impurity ions were taken to compare to neoclassical calculations. By using the force balance relation, we find that the differential poloidal flow of carbon and deuterium ions must be significantly larger than the prediction from the NCLASS model. Other models, such as NEO and GTC-NEO are closer to experimental observations, especially in regions of the plasma where the ion thermal diffusivity χ_i is close to neoclassical levels. By using the measured carbon poloidal rotation, the main-ion poloidal rotation can be inferred and compared to neoclassical theory. We find that the deuterium poloidal flow exceeds neoclassical estimates, being more ion-diamagnetic. A database of discharges with various levels of I_p and B_t was constructed, and it is found that the deuterium poloidal rotation becomes more

anomalous at low collisionality. The construction of E_r from main-ion contributions reveals that in the core of low rotation plasmas, E_r can be dominated by the poloidal rotation contribution.

In this article, we have presented the observation that the poloidal rotation of the main ions is consistently more rapid in the ion diamagnetic direction on DIII-D when the plasma is in the low collisionality "banana" regime. This conclusion was based on measurements of toroidal rotation profiles of the main-ions, and the requirement of satisfying radial force balance on a flux surface. A literature review also indicates that stronger ion diamagnetic flow is observed more commonly, when the poloidal flow deviates from neoclassical. Some such examples of this are seen from JET [8, 15] interior to a transport barrier, and NSTX [28, 53].

By removing the dependencies of main-ion poloidal flow on ion temperature gradient and magnetic field strength, a scaling of the effective dimensionless flow coefficient K_1 has been experimentally determined as a function of ion collisionality. Extrapolation to ITER collisionality reveals that the main-ion poloidal flow may significantly exceed the neoclassical estimates, with direct consequences on the magnitude of the radial electric field and its shear. Through a predictive TGYRO-TGLF simulation, the increased $\mathbf{E}\times\mathbf{B}$ shearing rate associated with anomalous poloidal flow reduces the turbulent ion thermal transport, resulting in an increased central ion temperature and improved performance.

Acknowledgments

This work supported in part by the U.S. Department of Energy under DE-FC02-04ER54698 and DE-AC02-09CH11466. The author gratefully acknowledges discussions with R.E. Bell, E.A. Belli, C. Chrystal, J.S. deGrassie, P.H. Diamond, D. Ernst, R.J. Groebner, T.S. Hahm, C. Holland and G.M. Staebler.

References

[1] Burrell K.H., 1997 *Phys. Plasmas* **4** 1499.
[2] Moyer R.A., Burrell K.H., Carlstrom T.N., Coda S., Conn R.W., Doyle E.J., Gohil P., Groebner R.J., Kim J., ad Lehmer R., 1995 *Phys. Plasmas* **2** 2397
[3] Politzer P.A. *et al* 2008 *Nucl. Fusion* **2** 075001
[4] Staebler G.M. and St John H.E., 2006 *Nucl. Fusion* **48** 075001
[5] Halpern F.D., Kritz A.H., Bateman G., Pankin A.Y., Budny R.V., and McCune D.C. 2008 *Phys. Plasmas* **15** 062505
[6] Kinsey J.E., Staebler G.M., Candy J., Waltz R.E., and Budny R.V. 2011 *Nucl. Fusion* **51** 083001
[7] Budny R.V., Andre R., Bateman G., Halpern F., Kessel C.E., Kritz A., and McCune D. 2008 *Nucl. Fusion* **48** 075005
[8] Crombé K. *et al* 2005 *Phys. Rev. Lett.* **95** 1
[9] Stix Thomas H. 1973 *Phys. Fluids* **16** 1260
[10] Morris R.C., Haines M.G., and Hastie R.J. 1996 *Phys. Plasmas* **3** 4513
[11] Marr K.D., Lipschultz B., Catto P.J., Mcdermott R.M., Reinke M.L., and Smiakov A.N. 2010 *Plasma Phys.* **52** 1
[12] Hassam A.B. and Antonesen T.M. 1994 *Phys. Plasmas* **1** 337
[13] Diamond P.H. and Kim Y.B. 1991 *Phys. Fluids B: Plasma Phys.* **3** 1626
[14] Hidalgo C., Silva C., Pedrosa M., Sánchez E., Fernandes H., and Varandas C. 1999 *Phys. Rev. Lett.* **83** 2203
[15] Tala T. *et al* 2007 *Nucl. Fusion* **47** 1012
[16] Hildago C. *et al* 2000 *Plasma Phys. and Controlled Fusion* **42** A153
[17] McDevitt C.J., Diamond, P.H., Güercan Ö.D. and Hahm T.S. 2010 *Phys. Plasmas* **17** 112509
[18] Hildago Carlos 2011 *Plasma Phys. and Controlled Fusion* **53** 074003
[19] Kim Y.B., Diamond P.H. and Groebner R.J. 1991 *Phys. Fluids B: Plasma Phys.* **3** 2050
[20] Field A.R., Mccone J., Conway N.J., Dunstan M., Newton S. and Wisse M. 2009 *Plasma Phys.* **51** 105002
[21] Brau K., Bitter M., Goldston R.J., Manos D., McGuire K. and Suckewer S. 1983 *Nucl. Fusion* **23** 1643
[22] Solomon W.M., Burrell K.H., Gohil P., Groebner R.J. and Baylor L.R. 2004 *Rev. Sci. Instrum.* **75** 3481
[23] Solomon W.M., Burrell K.H., Andre R., Baylor L.R., Budny R., Gohil P., Groebner R.J., Holcomb C.T., Houlberg W.A. and Wade M.R. 2006 *Phys. Plasmas* **13** 056116
[24] Bell R.E. and Feder Russell 2010 *Rev. Sci. Instrum.* **81** 10D724
[25] Camenen Y., Bortolon A., Karpushov A.N., Andrebe Y., Duval B.P., Federspiel L. and Sauter O. 2012 *Proceedings of 39th European Physical Society Conf. on Plasma Phys.*, Stockholm, Sweden, http://ocs.ciemat.es/epsicpp2012pap/html/author.html, Paper O5.116
[26] Chrystal C., Burrell K.H., Grierson B.A., Groebner R.J. and Kaplan D.H. 2012 *Rev. Sci. Instrum.* **83** 10D501
[27] Bell R.E. and Synakowski E.J. 2000 *AIP Conf. Proc.* **547** 39
[28] Bell R.E., Andre A., Kaye S.M., Kolesnikov R.A., Leblanc B.P., Rewoldt G., Wang W.X. and Sabbagh S.A. 2010 *Phys. Plasmas* **17** 082507
[29] Grierson B.A., Burrell K.H., Heidbrink W.W., Lanctot M.J. and Pablant N.A. 2012 *Phys. Plasmas* **19** 056107
[30] Kim J., Burrell K.H., Gohil P., Groebner R.J., Hinton F.L., Kim Y.B., Mandl W., Seraydarian R. and Wade M.R. 1994 *Plasma Phys.* **36** A183
[31] Grierson B.A., Burrell K.H., Chrystal C., Groebner R.J., Kaplan D.H., Heidbrink W.W., Munoz Burgos J.M., Pablant N.A., Solomon W.M. and Van Zeeland M.A. 2012 *Rev. Sci. Instrum.* **83** 10D529
[32] Seraydarian R.P., Burrell K.H., Brooks N.H., Groebner R.J. and Kahn C. 1986 *Rev. Sci. Instrum.*

57 155
[33] Gohil P., Burrell K.H., Groebner R.J. and Seraydarian R.P. 1990 *Rev. Sci. Instum.* **61** 2949
[34] Thomas D.M., McKee G.R., Burrell K.H., Levinton F., Foley E.L. and Fisher R.K. 2008 *Fusion Sci. & Technol.* **53** 487
[35] Houlberg W.A., Shaing K.C., Hirshman S.P. and Zarnstorff M.C. 1997 *Phys. Plasma* **4** 3230
[36] Belli E. and Candy J. 2008 *Plasma Phys.* **50** 095010
[37] Dif-Pradalier G., Diamond P.H., Grandgirard V., Sarazin Y., Abiteboul J., Garbet X., Ghendrih P., Latu G. Strugarek A. and Ku S. 2011 *Phys. Plasmas* **18** 062309
[38] Wang W.X., Tang W.M., Hinton F.L., Zakharov L.E., White R.B. and Manickam J. 2004 *Computer Physics Communications* **164** 178
[39] Kolesnikov R.A., Wang W.X., Hinton F.L., Rewoldt G. and Tang W.M. 2010 *Phys. Plasmas* **17** 022506
[40] Kim J., Burrell K.H., Gohil P., Groebner R.J., Kim Y.B., St John H.E., Seraydarian R.P. and Wade M.R. 1994 *Phys. Rev. Lett.* **72** 2199
[41] Bell R.E., Levinton F.M., Batha S.H., Snyakowski E.J. and Zarnstorff Michael 1998 *Phys. Rev. Lett.* **81** 1429
[42] Dif-Pradalier G., Grandgirard V., Sarazin Y., Garbet X. and Ghendrih Ph 2009 *Phys. Rev. Lett.* **103** 065002
[43] Waltz R.E., Staebler G.M., Candy J. and Hinton F.L. 2007 *Phys. Plasmas* **14** 122507
[44] Waltz R.E., Staebler G.M., Candy J. and Hinton F.L. Erratum [2007 *Phys. Plasmas* **14** 122507] 2009 *Phys. Plasmas* **16** 0879902
[45] Kolesnikov R.A., Wang W.X., Hinton F.L., Rewoldt G. and Tang W.M. 2010 *Plasma Phys. Controlled Fusion* **52** 042002
[46] Baylor L.R., Burrell K.H., Groebner R.J., Houlberg W.A., Ernst D.R., Murakami M. and Wade M.R. 2004 *Phys. Plasmas* **11** 3100
[47] St John H.E., Taylor T.S., Lin-Liu Y.R. and Turnbull A.D. 1995 *Plasma Phys. and Controlled Nucl. Fusion Research, Seville* International Atomic Energy Agency, Vienna, Vol. 3, p. 603
[48] deGrassie J.S., Rice J.E., Burrell K.H., Groebner R.J. and Solomon W.M. 2007 *Phys.Plasmas* **14** 056115
[49] Budny R.V., Yuan Xingqiu, Jardin S., Hammett G., Staebler G. and Kinsey J.E. 2012 "PTRANSP Tests of TGLF and Predictions for ITER" *Proceedings of 24th Fusion Energy Conf., San Diego, California* International Atomic Energy Agency, Vienna, Paper ITR/P1-29
[50] Staebler G.M., Kinsey J.E. and Waltz R.E. 2007 *Phys. Plasmas* **14** 055909
[51] Waltz R.E., Staebler G.M., Dorland William, Hammett G.W. and Kotschenreuther M. 1997 *Phys. Plasmas* **4** 2482
[52] Candy J. Holland C., Waltz R.E., Fahey M.R. and Belli E. 2009 *Phys. Plasmas* **16** 060704
[53] Kaye S., Bell R., Gates D., Leblanc B., Levinton F., Menard J., Mueller D., Rewoldt G., Sabbagh S., Wang W. and Yuh H. 2007 *Phys. Rev. Lett.* **98** 175002

Figure 1. Profiles of density, temperature, toroidal rotation and differential toroidal rotation for ECH H-mode. Monte-Carlo error bars included for region where main-ion measurements are available. Differential toroidal rotation includes prediction of deuterium rotation from various neoclassical models.

Figure 2. Differential poloidal rotation (a), carbon (b) and deuterium (c) V_θ, and E_r (d) for the profiles in figure 1. Error bars on NCLASS results are from Monte-Carlo perturbation. (e) Displays the significance of all three components when forming the radial electric field.

Figure 3. Scaling of differential toroidal rotation between deuterium and carbon over a range of collisionality

Figure 4. (a) Comparison of measured differential poloidal flow (that does not depend on measuring V_θ^D or V_θ^C directly) to neoclassical calculations. (b) Main-ion poloidal flow.

Figure 5. Variation of K_1 with ion collisionality.

Figure 6. (a) Radial electric field from ITER case 20100N05 at 245 seconds and (b) modified with enhanced poloidal rotation in accordance with the experimental scaling of figure 5.

Figure 7. Long wavelength ion growth rates compared to $\mathbf{E}\times\mathbf{B}$ shear rates for radial electric field from ITER case 20100N05 at 245 seconds and modified with enhanced poloidal rotation.

Figure 8. TGYRO-TGLF result for original $\mathbf{E}\times\mathbf{B}$ shearing rates from PTRANSP 20100N05, and with modified radial electric field. Ion and electron (inset) temperatures increase as poloidal flow coefficient K_1 is increased above the NCLASS value.

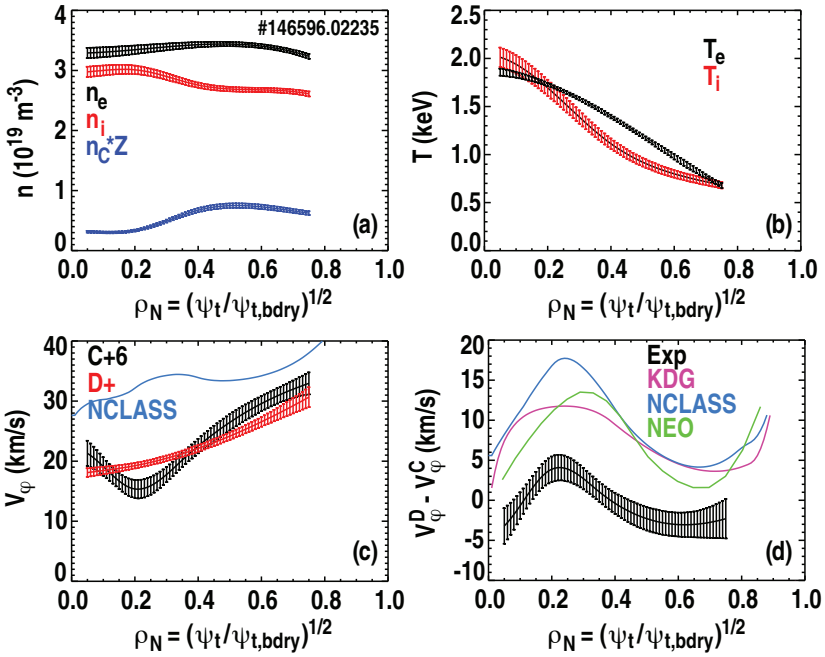

B.A. Grierson Figure 1

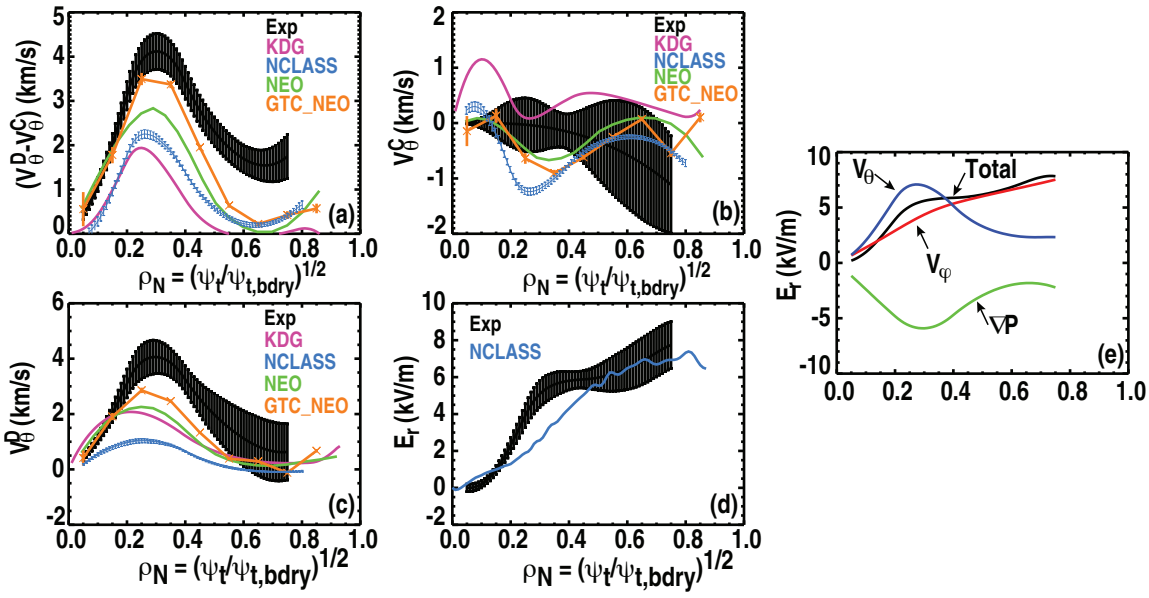

B.A. Grierson Figure 2

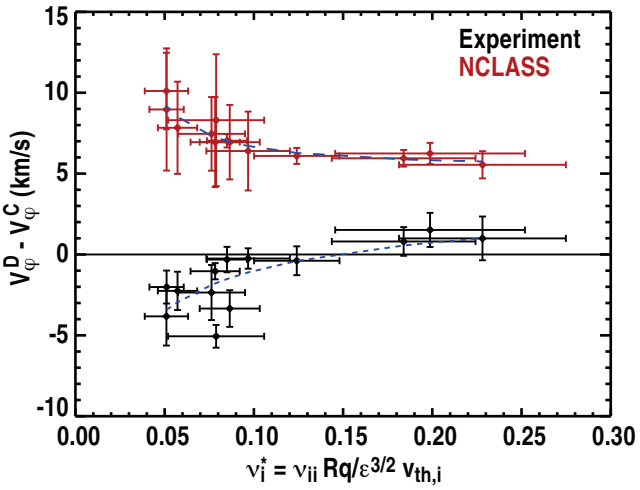

B.A. Grierson Figure 3

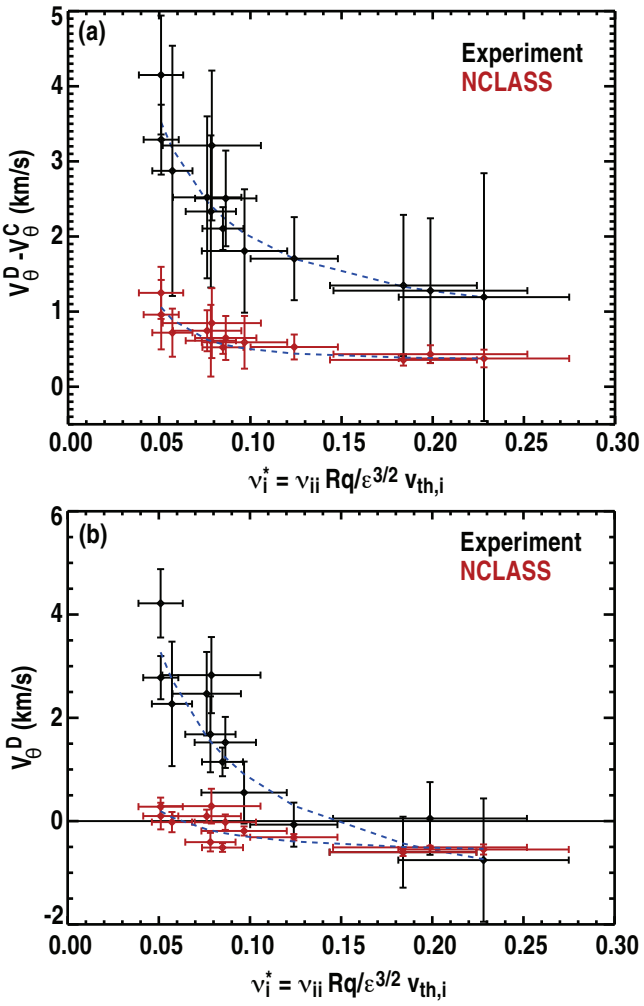

B.A. Grierson Figure 4

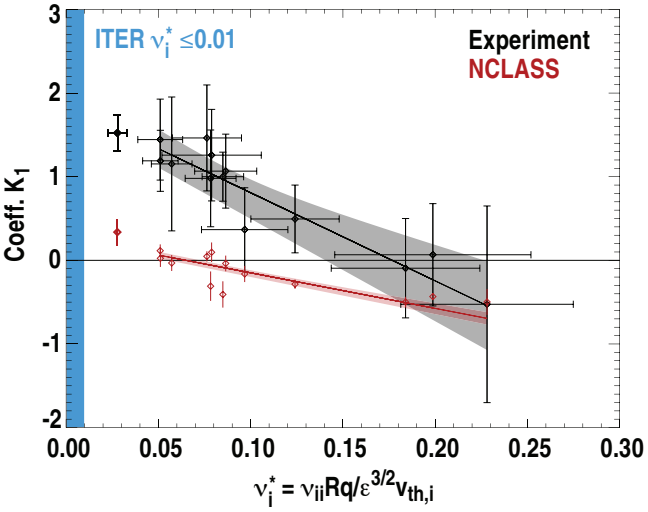

B.A. Grierson Figure 5

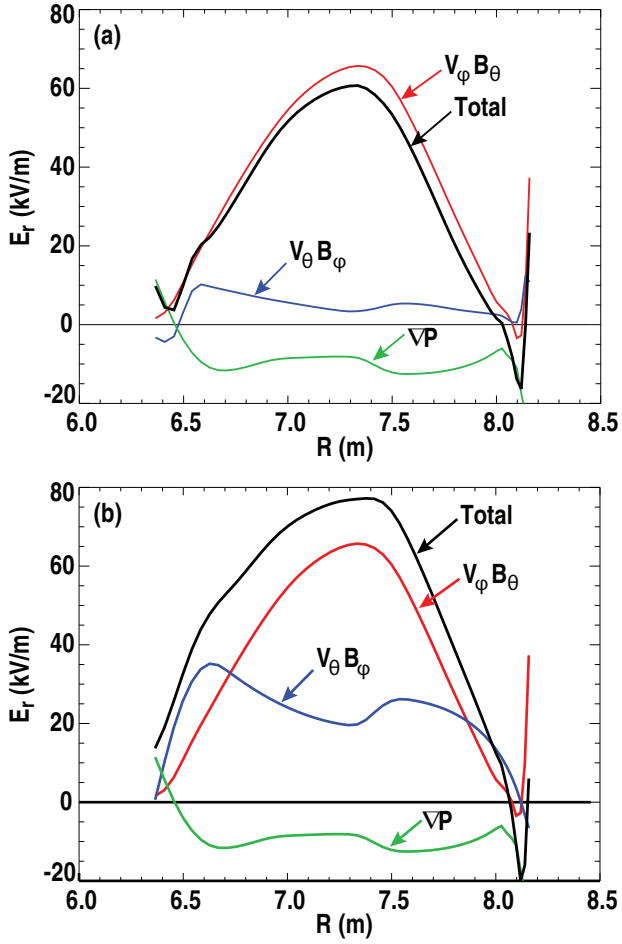

B.A. Grierson Figure 6

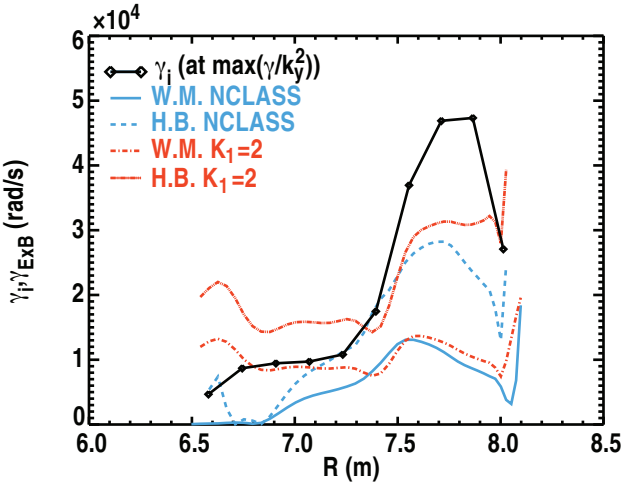

B.A. Grierson Figure 7

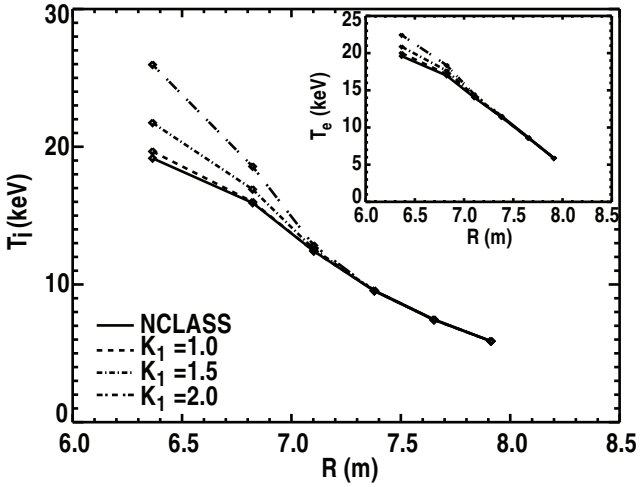

B.A. Grierson Figure 8

The Princeton Plasma Physics Laboratory is operated
by Princeton University under contract
with the U.S. Department of Energy.

Information Services
Princeton Plasma Physics Laboratory
P.O. Box 451
Princeton, NJ 08543

Phone: 609-243-2245
Fax: 609-243-2751
e-mail: pppl_info@pppl.gov
Internet Address: http://www.pppl.gov